A&A 410, 649–661 (2003)
DOI: 10.1051/0004-6361:20031241

Astronomy & Astrophysics

2MASS J0516288+260738: Discovery of the first eclipsing late K + Brown dwarf binary system?⋆,⋆⋆,⋆⋆⋆

S. L. Schuh[1,14,†], G. Handler[2,3], H. Drechsel[4], P. Hauschildt[5], S. Dreizler[1,14,†], R. Medupe[3,6], C. Karl[4,†], R. Napiwotzki[4,†], S.-L. Kim[7], B.-G. Park[7], M. A. Wood[8], M. Paparó[9], B. Szeidl[9], G. Virághalmy[9], D. Zsuffa[9], O. Hashimoto[10], K. Kinugasa[10], H. Taguchi[10], E. Kambe[11], E. Leibowitz[12], P. Ibbetson[12], Y. Lipkin[12], T. Nagel[1,†], E. Göhler[1,†], and M. L. Pretorius[13]

[1] Institut für Astronomie und Astrophysik, Universität Tübingen, Sand 1, 72076, Tübingen, Germany
e-mail: schuh@astro.uni-tuebingen.de
[2] Institut für Astronomie, Universität Wien, Türkenschanzstraße 17, 1180 Wien, Austria
[3] South African Astronomical Observatory, PO Box 9, Observatory 7935, Cape, South Africa
[4] Dr.-Remeis-Sternwarte, Astronomisches Institut der Universität Erlangen-Nürnberg, Sternwartstr. 7, 96049 Bamberg, Germany
[5] Hamburger Sternwarte, Universität Hamburg, Gojenbergsweg 112, 21029 Hamburg, Germany
[6] Department of Physics, University of the North-West, Private Bag X2046, Mmabatho 2735, South Africa
[7] Korea Astronomy Observatory, 61-1, Whaam, Yuseong, Daejeon, 305-348, Korea
[8] Department of Physics and Space Sciences and SARA Observatory, Florida Institute of Technology, 150 West University Boulevard, Melbourne, FL 32901-6975, USA
[9] Konkoly Observatory, Box 67, 1525 Budapest XII, Hungary
[10] Gunma Astronomical Observatory, 6860-86 Nakayama Takayama-mura Agatsuma-gun Gunma-ken, Postal Code: 377-0702, Japan
[11] Department of Earth and Ocean Sciences, National Defense Academy, Yokosuka, Kanagawa 239-8686, Japan
[12] Wise Observatory, Sackler Faculty of Exact Sciences, Tel Aviv University, Tel Aviv 69978, Israel
[13] Department of Astronomy, University of Cape Town, Rondebosch 7700, South Africa
[14] Universitätssternwarte Göttingen, Geismar Landstraße 11, 37083 Göttingen, Germany

Received 8 April 2003 / Accepted 4 August 2003

Abstract. We report the discovery of a new eclipsing system less than one arcminute south of the pulsating DB white dwarf KUV 05134+2605. The object could be identified with the point source 2MASS J0516288+260738 published by the Two Micron All Sky Survey. We present and discuss the first light curves as well as some additional colour and spectral information. The eclipse period of the system is 1.29 d, and, assuming this to be identical to the orbital period, the best light curve solution yields a mass ratio of $m_2/m_1 = 0.11$, a radius ratio of $r_2/r_1 \approx 1$ and an inclination of 74°. The spectral anaylsis results in a $T_{\rm eff} = 4200$ K for the primary. On this basis, we suggest that the new system probably consists of a late K + Brown dwarf (which would imply a system considerably younger than ≈0.01 Gyr to have $r_2/r_1 \approx 1$), and outline possible future observations.

Key words. ephemerides – stars: variables: general – stars: binaries: eclipsing – stars: low-mass, brown dwarfs – stars: individual: 2MASS J0516288+260738

Send offprint requests to: S. L. Schuh,
e-mail: Schuh@astro.uni.tuebingen.de

⋆ This paper uses observations made at the Bohyunsan Optical Astronomy Observatory of Korea Astronomy Observatory, at the South African Astronomical Observatory (SAAO), at the 0.9 m telescope at Kitt Peak National Observatory recommissioned by the Southeastern Association for Research in Astronomy (SARA), at Gunma Astronomical Observatory established by Gunma prefecture, Japan, at the Florence and George Wise Observatory, operated by the Tel-Aviv University, Israel and at Piszkéstető, the mountain station of Konkoly Observatory of the Hungarian Academy of Science, Hungary.

⋆⋆ This publication makes use of data products from the Two Micron All Sky Survey, a joint project of the University of Massachusetts and the Infrared Processing and Analysis Center / California Institute of Technology, funded by the National Aeronautics and Space Administration and the National Science Foundation.

⋆⋆⋆ The Digitized Sky Survey was produced at the Space Telescope Science Institute under US Government grant NAG W-2166. The images of these surveys are based on photographic data obtained using the Oschin Schmidt Telescope on Palomar Mountain and the UK Schmidt Telescope. The plates were processed into the present compressed digital form with the permission of these institutions.

† Visiting Astronomer, German-Spanish Astronomical Centre, Calar Alto, operated by the Max-Planck-Institute for Astronomy, Heidelberg, jointly with the Spanish National Commission for Astronomy.

1. Introduction

Detached eclipsing binaries provide precise fundamental stellar parameters like mass and radius and are thus the prerequisite for the validation of stellar evolutionary models. The empirical constraints from over four dozen systems have shown that for main sequence stars between 1 and 10 $M_\odot$ the agreement is acceptable, i.e. better than 2% (Andersen 1991, 1998), while at the lower main sequence the situation is far less satisfying. Up to now, only three eclipsing systems with M-type primaries are known, despite the fact that low mass main sequence stars dominate the stellar population by number. The first such system to be discovered was YY Gem (Joy & Sanford 1926; van Gent 1926), followed by CM Dra (Eggen & Sandage 1967, and references therein) and CU Cnc (Delfosse et al. 1999); first mass determinations came from Leung & Schneider (1978), Lacy (1977) and Delfosse et al. (1999), respectively. While Metcalfe et al. (1996) find the slope of the mass-radius relation derived from the M dwarf binary system CM Dra in agreement with model predictions, Delfosse et al. (2000) reported on a disagreement between empirical and theoretical mass-luminosity relations of 10–20% in the V band, and recent precise analyses of YY Gem (Torres & Ribas 2002) and CU Cnc (Ribas 2003) also revealed an underestimation (10–20%) of the radii of low mass stars from current evolutionary models. Additional constraints for the empirical mass-radius relation are provided by the first interferometric measurements of radii from lower main sequence stars (Ségransan et al. 2003). These results agree well with model predictions at the present accuracy level, with a possible discrepancy for stars with 0.5–0.8 $M_\odot$. Such observations do not provide an independent measurement of the stellar mass, however, so that eclipsing systems still are the primary source for a model-independent determination of fundamental parameters.

Future improvements of the theoretical mass-radius relation for the lower main sequence would strongly benefit from a larger empirical database through an increased sample of eclipsing binaries. Recently, 137 eclipsing low-luminosity candidates were announced by the OGLE (Optical Gravitational Lensing Experiment) consortium (Udalski et al. 2002a,b, 2003), of which several of the secondaries turned out to be M-type stars (Dreizler et al. 2002). In this paper we report the discovery of another interesting eclipsing binary system, 2MASS J0516288+260738, whose components appear to bracket the M-star range, with the potential of extending the empirical mass-radius relation into the sub-stellar range.

The new eclipsing system has been discovered in observational data taken during a coordinated photometric monitoring campaign in December 2001. This dataset has been obtained to monitor the light variations of the DB variable white dwarf KUV 05134+2605 (Grauer et al. 1989; Handler et al. in prep.). It consists of many individual light curves taken by either photomultiplier (PMT) or CCD instruments; the newly discovered object is included in 48 individual time series of images obtained with CCD cameras. While analysing field stars for photometric stability to check whether they could be used as references, an object located a little less than one arcminute south of the DB was found to show the signature of an eclipse in the Calar Alto 2.2 m data set of 2001 Dec. 07 (see Table 1, only available in electronic form at `http://www.edpsciences.org`). Subsequent searches in the other data sets revealed that eight more eclipses had partly or fully been observed. A year later, 5 additional data sets were obtained, two of which covered the eclipse. The full time-resolved photometric data are compiled in Sect. 3. Archive searches contributed an identification of the object as well as additional colour information (Sects. 2 and 4). Two months after the initial observations, an optical spectrum could be obtained, and in the following observing season, an infrared spectrum was taken (see Sect. 4).

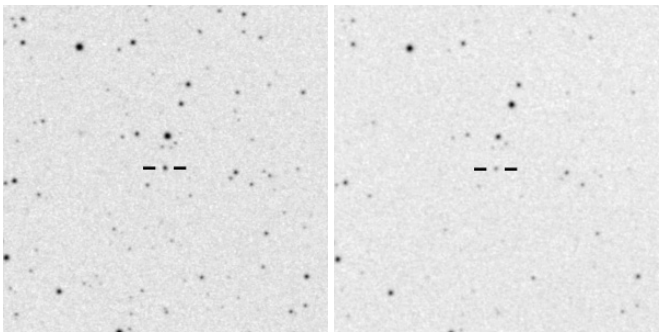

Fig. 1. Finding charts for 2MASS J0516288+260738 (DSS-2 red: left, DSS-2 blue: right). The side length is $4' \times 4'$ for each image; north is up and east is to the right.

In the following, we compile the information that is currently available on the object, report our results from the light curve solution and the spectral analysis, and propose a possible configuration for this system.

2. Positional information

A search with SIMBAD yielded no catalogued object at or near the coordinates of the eclipsing object, but loading the Incremental Release Extended Source Catalog of the Two Micron All Sky Survey (2MASS) into ALADIN resulted in a match. We could clearly identify our object with the point source 2MASS J0516288+260738, and later with a point source in the USNO-*B* catalogue (cf. Sect. 4.1). We use the 2MASS catalog entry to give improved coordinates: RA = $05^{\rm h}16^{\rm m}28\overset{\rm s}{.}81$, $\delta = +26^\circ07'38\overset{''}{.}8$ (J2000). For a clear identification, the object is marked with horizontal bars in the finding charts given in Fig. 1.

3. The light curve

3.1. Time-resolved photometric data

All photometric data sets obtained with CCD cameras in the December 2001 KUV 05134+2605 campaign were compiled. Additional observations obtained in November 2002 were added later. A list of all data sets used is given in Table 1, with a complementary key to the observing sites involved in Table 2. All data were bias and flatfield corrected according to standard routines. Aperture photometry was performed on all of these frames using the TRIPP package (Schuh et al. 2003).

Table 2. Key to observatory sites.

Site		Telescope	Observers
CAHA	Calar Alto Observatory, Centro Astronómico Hispano Alemán, Almería, Spain	2.2 m	SD, SLS
CAHA II	Calar Alto Observatory, Centro Astronómico Hispano Alemán, Almería, Spain	1.2 m	TN, EG
BOAO	Bohyunsan Optical Astronomy Observatory, Korea	1.8 m	SLK, BGP
SAAO	South African Astronomical Observatory, Sutherland, South Africa	1.0 m	GH, TM
SARA	Kitt Peak National Observatory, Tucson, Arizona, United States of America	0.9 m	MW
GAO	Gunma Astronomical Observatory, Japan	1.5 m	OH, KK, HT, EK
WISE	The Florence and George Wise Observatory, Tel-Aviv University, Israel	1.0 m	EL, PI, YL
Piszkéstető	Piszkéstető, the mountain station of Konkoly Observatory, Mátra Mountains, Hungary	1.0 m	MP, BS, GV, DZ

Two reference stars that are available on all frames (shown to be stable during the whole 2001 campaign) were chosen and used consistently for all data sets to produce relative light curves. The total light curve was then scaled by a unique factor to produce a light curve with a mean relative intensity of unity for the white light contributions outside eclipse. Finally, all times were converted from Julian date (JD) to heliocentrically corrected Julian date (HJD). The result is shown in Fig. 2.

The light curve shows a clear periodicity of 1.29 days. All observed eclipses are similar to each other, have a duration of about 0.10 days and exhibit a decrease in flux of 15% (or 0.17 mag) at the deepest point. There is no indication of a secondary eclipse in any of the eight 2001 data sets that partly or fully cover the phase where such an event would be expected. Furthermore, the three 2002 data sets covering that phase put a clear upper limit to the depth of any secondary eclipse: 0.49% (or 5.4 mmag) in white light and 0.70% (or 7.6 mmag) in the Johnson *I* filter.

3.2. Ephemeris

Primary minima times were determined by fitting parabolas to the eclipses. The results for the epochs 0 (two independent data sets), 3, 9, 10, 11, 12 (concatenated from two different non-overlapping data sets), 259 and 262 are given in Table 1; no fits could be obtained for epochs 5 and 7 since only parts of either ingress or egress had been observed there. A linear regression for the measured minima times then gives the linear elements and their 1σ errors for the primary minima as

$$\begin{array}{rcl} \mathrm{HJD} = 2\,452\,251\overset{\mathrm{d}}{.}5173 & + & 1\overset{\mathrm{d}}{.}29395 \cdot E. \\ \pm 16 & & \pm 25 \end{array}$$

This ephemeris was used to generate a folded profile from the data taken in 2001.

The folded profile has also been carefully inspected to verify that no secondary eclipse is apparent in the data. The profile remains at the same relative flux level outside of the primary eclipse with no significant indication of ellipsoidal light variations or reflection effects. It was then used to obtain a light curve solution as discussed in Sect. 6.

4. Colour and spectral information

4.1. Colours

To derive a visual magnitude for the analysed object, we have obtained further photometry of the field. The observations were made at the South African Astronomical Observatory's 30″ telescope using the UCT CCD Photometer. A series of 10 images was taken in a Johnson *V* filter on March 10 2003 starting at 18:19:03 UT (exposure time 100 s). The measurements were thus made out of eclipse. We compare our results for KUV 05134+2605 and 2MASS J0516288+260738 to estimate that the mean *V* magnitude difference (KUV − 2MASS) is $1.44^{\mathrm{m}} \pm 0.02$. Due to the rapid nature of the variations in the DB variable, it is not a problem to derive a good mean magnitude for that object. Using $V = 16.70$ (Wegner et al. 1990) for KUV 05134+2605, we obtain $V_{2\mathrm{MASS}} = 18.1^{\mathrm{m}} \pm 0.1$.

Table 3. Johnson *V*, USNO-*B B*, *R*, *I* and 2MASS *J*, *H*, *K* magnitudes.

	B	*V*	*R*	*I*	*J*	*H*	*K*
Magnitude	19.47	18.1	16.8	15.84	14.247	13.346	13.115
Error	±0.3	±0.1	±0.3	±0.3	±0.040	±0.039	±0.039
λ_0 [μm]	0.43	0.55	0.70	0.90	1.25	1.65	2.17
F_{ν_0}[Jy]	4440	3810	2880	2240	1593	1089	713
F_λ [∗]	1.17	2.17	3.36	3.83	6.12	5.51	2.58

∗ $\left[\mathrm{erg\,s^{-1}cm^{-2}\AA^{-1}} \times 10^{-16}\right]$.

Photographic *B*, *R* and *I* magnitudes are published in the USNO-*B* catalogue (Monet et al. 2003), and infrared *J*, *H* and *K* magnitudes are available from the 2MASS catalog. They are compiled in Table 3. The USNO-B and 2MASS magnitudes *m* have been converted to F_λ using the relation

$$F_\lambda\left[\mathrm{erg\,s^{-1}cm^{-2}\AA^{-1}}\right] = F_{\nu_0}[\mathrm{Jy}] \cdot 10^{-0.4m} \cdot 3 \times 10^{-13} / \lambda_0[\mu\mathrm{m}]^2.$$

The photometric zero points F_{ν_0} and central wavelengths λ_0 used for the conversion are tabulated in Table 3 along with the results for F_λ. For the 2MASS filters, these quantities were obtained from Squires et al. (2002), while for the white light we used the values published for *V* by Campins et al. (1985) and Rieke et al. (1985) for the Johnson *UBVRI*+ system.

The Sloan Digital Sky Survey (SDSS) does not cover the field in its EDR (Early Data Release, Stoughton et al. 2002) so that no further photometric information is available. Since the object, according to its infrared colours, is very red, we also checked the VLA FIRST survey at 20 cm, which currently does not cover this field either, and the NRAO/VLA Sky Survey (NVSS) at 1.4 GHz (Condon et al. 1998), which covers the field but does not show a radio source in the vicinity. For completeness, we finally note that neither the ROSAT Bright Source Catalogue as compiled from the WFC All Sky Survey (Pounds et al. 1993) nor the ROSAT XUV Pointed

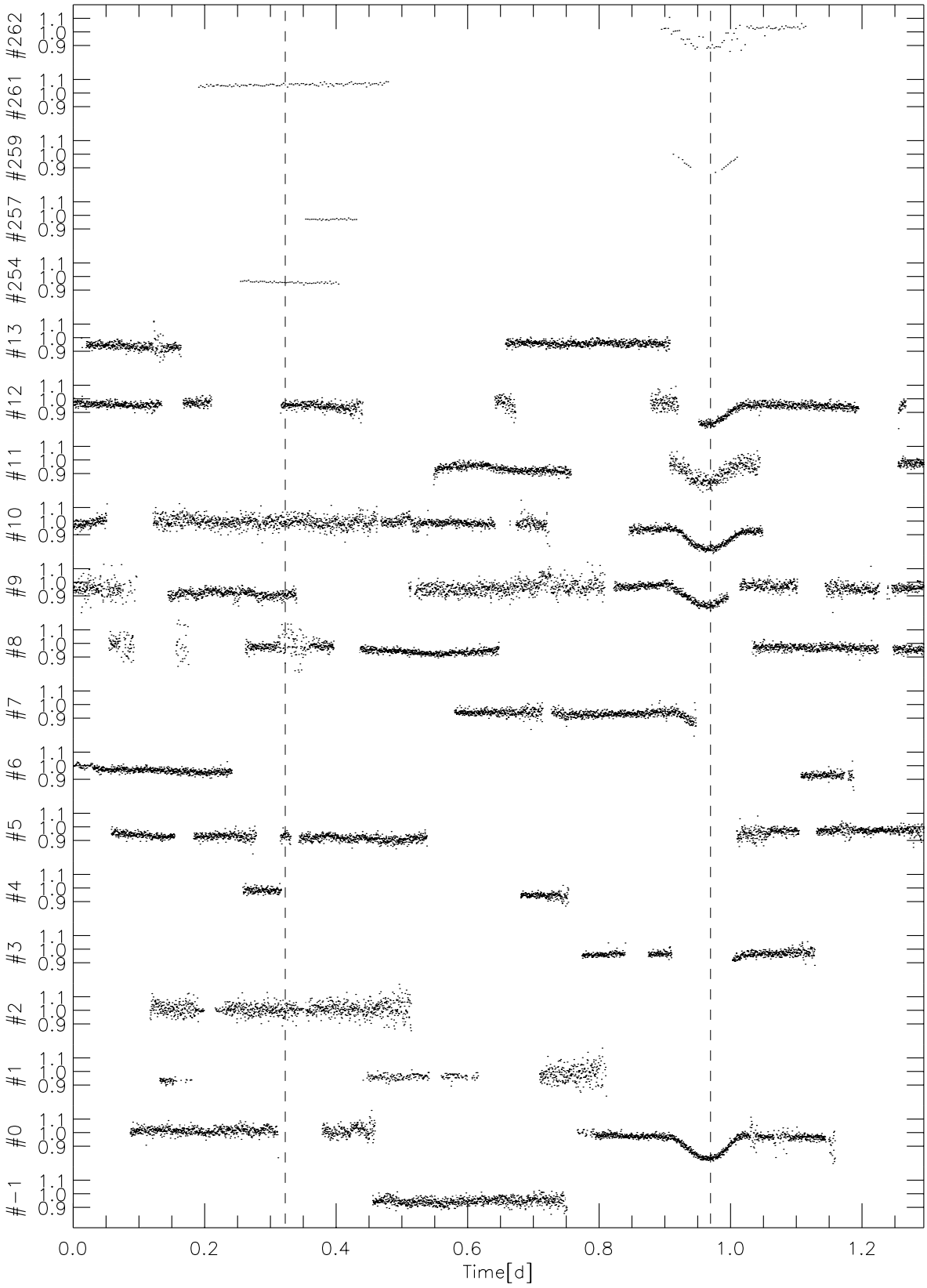

Fig. 2. Overview of the photometric observations; the flux is given in fractional intensity units. Time is in days, with data binned into units of 30 s. Time increases from left to right and from bottom to top. The epochs (labelled #*n*) are displayed continuously up to the end of the 2001 campaign, while for the 2002 observations only those epochs were included in the plot for which data points exist. The primary eclipse is displayed at multiples of 0.97 d to place it at a phase of 0.75 in this plot, allowing convenient viewing of both phase 0.25 where the secondary minima would be located as well as of the primary eclipses (both marked by horizontal dashed lines). The scatter in the individual light curves contributed by different sites varies according to aperture, actual exposure time and weather conditions.

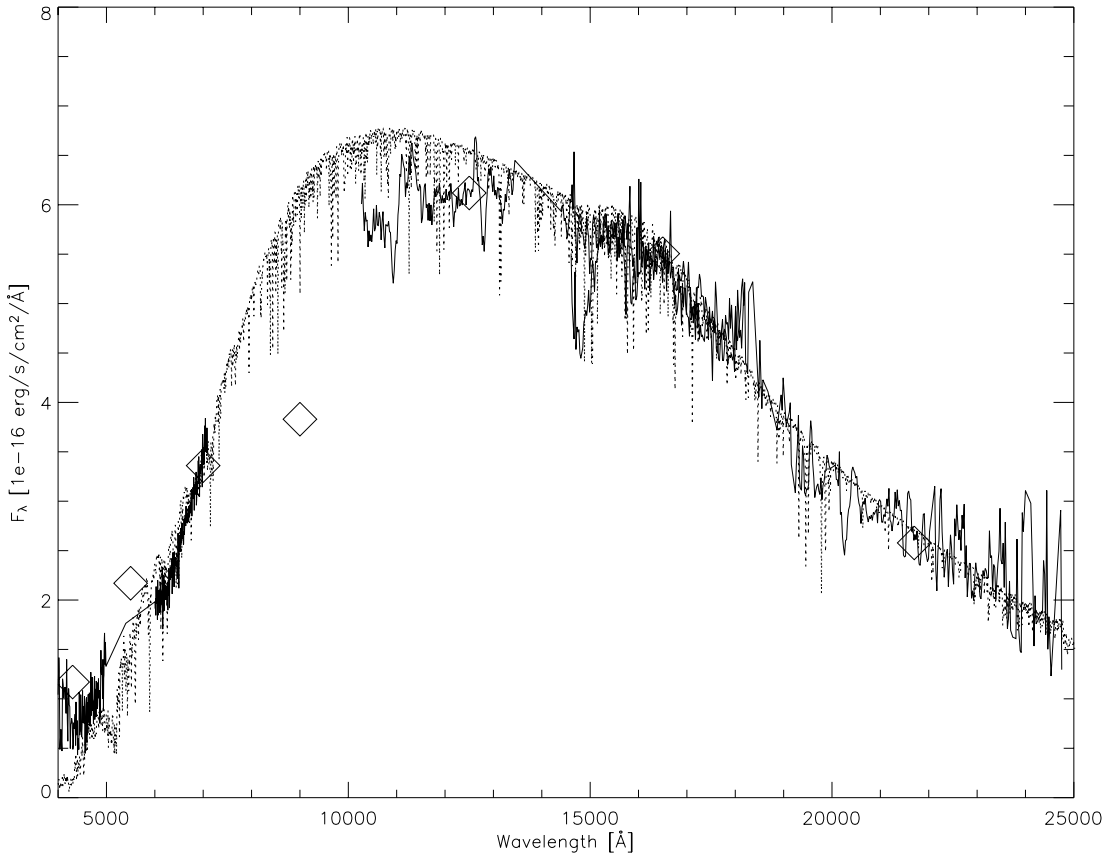

Fig. 3. Measured flux calibrated optical and IR spectra (solid line), Johnson *V*, USNO-*B* and 2MASS colours converted to F_λ (diamond symbols), in comparison with the best fit model spectrum (dotted). For details see text.

Phase Source Catalogue as compiled from WFC observations during pointed phase (Kreysing et al. 1995) list sources at or near the object's position.

4.2. Optical spectra

Two medium resolution spectra of 2MASS J0516288+260738 were obtained in February 2002 at the Calar Alto 3.5 m telescope with the double beam spectrograph TWIN (see Table 4, first part). Gratings # 5 and # 6 were used for the blue and red arm, respectively, with the dichroic set at 550 nm. Together with slit widths of 1.″2 and 1.″5 for the first and second exposure, this resulted in spectral resolutions of 0.94 and 1.04 Å. Both spectra turned out later on to have been taken well outside any eclipse, but only the spectrum taken on February 25 reaches an exposure level acceptable for further analysis: the signal-to-noise level per pixel for the first spectrum is only 3, but reaches 8 for the second one. The frame and corresponding wavelength calibration frame were bias and flatfield corrected. Then the spectrum was extracted, sky corrected, subjected to a cosmic ray filtering, corrected for the illumination function, and finally wavelength calibrated. Flux calibration was done by first applying the same procedure to an exposure of the standard star G191-B2B taken in the same night, then using tabulated flux values to do the absolute calibration. The two resulting optical spectra in the wavelength ranges of 3900–5000 Å and 6000–7090 Å of 2MASS J0516288+260738 are displayed in Fig. 3 (rescaling as described in Sect. 5). At the given S/N ratio, no lines or features, in particular no TiO bands, can be discerned.

4.3. Infrared spectra

By the start of the following observing season for 2MASS J0516288+260738 in autumn 2002, the compilation and reduction of the light curve was not only complete enough to allow the prediction of eclipse times, but also to attempt a first light curve solution, based on an estimate of the spectral class obtained from the slope of the optical spectrum. This confirmed the suspicion that the system might be made up from two low mass stars or a low mass star and a substellar object, and therefore justified taking infrared spectra during Director's discretionary time at Calar Alto Observatory. An *H* and *K* band spectrum was observed in October 2002, and a *J* and *H* band spectrum in February 2003.

Each time, a set of 24 spectra was obtained using the OMEGA-Cass instrument mounted on the 3.5 m telescope (see Table 4), well off both primary and secondary eclipse. Since the background is high for infrared observations, the set of 24 spectra was obtained in such a way that alternating exposures contain the source on two different locations on the chip. After bias and flatfield correction of the individual exposures, this allows to determine a mean background at the (dispersed) location of the source for both types of images from the

Table 4. Spectroscopic observations.

Object	Instrument	λ range [Å]	Start time (UT)		Exp. time	HJD
2MASS J0516288+260738	TWIN	3900–5000, 6000–7090	2002 Feb. 23	21:34	1800 s	2 452 329.411
G191-B2B	TWIN	3900–5000, 6000–7090	2002 Feb. 25	18:40	300 s	2 452 331.281
2MASS J0516288+260738	TWIN	3900–5000, 6000–7090	2002 Feb. 25	20:49	1800 s	2 452 331.380
2MASS J0516288+260738	OMEGA-Cass	*HK*: 14 000–25 000	2002 Oct. 27	23:31	24×120 s	2 452 575.484
GD 71	OMEGA-Cass	*HK*: 14000–25000	2002 Oct. 28	02:21	10×120 s	2 452 575.602
2MASS J0516288+260738	OMEGA-Cass	*JH*: 10 000–18 000	2003 Feb. 03	21:49	24×120 s	2 452 674.412
GD 71	OMEGA-Cass	*JH*: 10 000 – 18 000	2003 Feb. 03	23:12	24×120 s	2 452 674.470

respective subset of the complementary frames. These two measures of the mean background can then be used to subtract the appropriate background from all frames of the two subsets. To do this, the shift for each background row was first determined by cross-correlating it along the dispersion direction with the corresponding image row, and the overall run of the shift along the chip obtained by fitting these row-by-row measurements with a low-order polynomial. To achieve the best possible subtraction in the vicinity of the source location on the chip, this fit with sub-pixel accuracy was then used to shift the background onto the image before subtracting it. For the wavelength dispersions at the two source locations, no shifts could be detected during the course of the exposure series. Therefore, next these bias subtracted, flatfield corrected and background subtracted frames of each of the two sets were added to yield two summed images. The spectra were extracted from these two images using standard procedures for extraction, sky correction, cosmic filtering, illumination correction, and wavelength calibration. The same procedure was used for the set of 10 and 24 exposures of the standard star GD 71. For each observation, the two spectra for the standard star were then combined and compared to tabulated flux values to obtain the factor for absolute flux calibration, which was then applied to both the two object spectra and the two individual standard star spectra.

Comparing the results for the individual spectra for both stars leads to the conclusion that the error bars in the resulting combined spectra must be considered to be of the same magnitude as any "features" that one might be tempted to spot.The same conclusion results from a comparison of the *H* band parts of the spectra from the two different observing dates, where most "features" are not reproduced. Furthermore, a flux difference by a factor of about 1.5 between those two independent observations gives an estimate for the errors in the flux calibration. The rescaled infrared spectra for 14 000–25 000 Å and 10 000–18 000 Å are displayed in Fig. 3.

5. Spectral analysis

The flux calibrated optical and infrared spectra as well as the broad band filter measurements converted to flux values (diamond symbols) are all displayed together in Fig. 3. To obtain a consistent image of the spectral energy distribution, the magnitude measurements were used to rescale the spectra where necessary. A unique correction factor was applied to both optical spectra simultaneously, and a correction factor was applied to each of the two independent infrared spectra (*HK* and *JH*).

The uncertainty in the optical spectrum results since both object and flux standard star were observed under non-photometric conditions. The same argument applies to the infrared spectral observations, where observations from different nights, although both nominally flux calibrated, result in different flux levels for the overlapping *H* band. A consistent adjustment therefore seems justified. Residual errors may result from the transformation of magnitudes to F_λ.

In the following, it will be assumed that the observed spectral energy distribution consists of light from the primary only; furthermore, for reasons detailed in Sect. 7.2, the primary will be presumed to be a late main sequence star. Since 2MASS J0516288+260738 is located close to the galactic plane, the effect of interstellar reddening is not negligible even for low-luminosity and close-by objects.

For the initial analysis of the observed data we use a grid of model atmospheres and synthetic spectra that is based on the models of Allard et al. (2001). We have extended the model grid to effective temperatures of 10 000 K for gravities from $5.5 \leq \log g \leq -0.5$ using spherical symmetry. The mixing length was set to twice the pressure scale height, this choice of the mixing length was calibrated on early M dwarfs (Ludwig et al. 2002).

Synthetic spectra generated from the models were compared to the observed spectra using an IDL program. This step was restricted to the infrared spectra. First, the resolution of the synthetic spectra was degraded to that of each observed spectrum by convolution with a Gaussian of the appropriate width, and the spectra were normalized to unit area for scaling. Next, for each observed spectrum the program calculated a quality function q, similar to a χ^2 value, for the comparison with all synthetic spectra in the grid. The quality function is calculated by first scaling the model spectrum to the observed fluxes and then by mapping the synthetic spectrum (reduced to the resolution of the observed data) onto the grid of observed wavelength points and then calculating

$$q = \sum_i w_i \left(0.5 \frac{f_i^{\rm model} - f_i^{\rm obs}}{f_i^{\rm model} + f_i^{\rm obs}} \right)^2$$

with $w_i = 0.5(f_{i+1}^{\rm obs} + f_i^{\rm obs})(\lambda_{i+1}^{\rm obs} - \lambda_i^{\rm obs})$ where $f^{\rm model}$ is the (mapped) flux of the model spectrum, $f^{\rm obs}$ is the observed flux,

and $\lambda^{\rm obs}$ the observed wavelength. For each model, this procedure was repeated for $0.0 \leq E(B-V) \leq 2.5$ in steps of 0.1 to independently determine the reddening. For this procedure, we used the reddening model of Cardelli et al. (1989). We then selected the models that resulted in the 3–10 lowest q values as the most probable parameter range for each individual star. The "best" value was chosen by visual inspection, at this point additionally considering the optical spectra to ensure a consistent fit. This procedure allows a rough estimate of the uncertainty in the stellar parameters. Note that it does not eliminate systematic errors in the stellar parameters due to missing, incorrect or incomplete opacity sources. The comparison was done for a total of 377 model atmospheres with solar abundances in the range $2000\,{\rm K} \leq T_{\rm eff} < 5000\,{\rm K}$ and $5.5 \leq \log g \leq 0.0$. Together with the search range in extinction this leads to 7539 combinations that were considered in the procedure. With the exception of allowing the extinction to vary this is the same procedure that was used in Leggett et al. (2001) and Leggett et al. (2002).

The best fitting model has an effective temperature $T_{\rm eff} = 4200\,{\rm K}$ and a reddening of $E(B-V) = 0.9$. The low resolution of the data and the relative insensitivity of the spectral energy distribution to gravity prevent us from determining a value of $\log g$, it is clear, however, that the object is a dwarf rather than a giant. The formal error in effective temperature is about ±200 K and about ±0.2 for the extinction. The low resolution data also prevent detailed metallicity determinations, and so far only solar metallicities were considered. Overall, the spectral analysis results suggest a spectral type of about K7 V (±2 subclasses).

The resulting fit is shown in Fig. 3. We have applied the reddening to the synthetic spectrum (dotted line) in order to facilitate the comparison without modifying the data themselves. All available spectral and colour information is included in the figure. The fit is in general acceptable, unfortunately data are missing in spectral regions where they would be extremely useful to test the resulting model parameters.

A consistency check of our solution can be performed by comparing our measured reddening with the model of the Galactic interstellar extinction constructed by Arenou et al. (1992). First we estimate the distance from the spectral type – absolute magnitude calibration of Schmidt-Kaler (1982). From their Table 13 we get an absolute magnitude of $M_V = 8.1$ for spectral type K7 V. With $E(B-V) = 0.9$ as derived above, the dereddened V magnitude is 15.3 (adopting $R = 3.1$). Thus the resulting distance module is 7.2, corresponding to a distance of 280 pc. The reddening predicted from the Arenou et al. model and the position of 2MASS J0516288+260738 ($l = 178.8$, $b = -6.9$) amounts to $E(B-V) = 0.48 \pm 0.24$. The scatter results mostly from the patchiness of the interstellar medium in this region. Although this value is somewhat smaller than our measured reddening both values agree within the error limits. Note that the model of Galactic extinction provides an upper limit of $E(B-V) = 0.72 \pm 0.36$ for the reddening at the position of 2MASS J0516288+260738. This limit results from the fact that stars exceeding a certain distance are above the absorbing dust layers of the Galaxy. This allows us to rule out highly reddened early type stars (cf. also the independent discussion of this aspect in Sect. 7.2 which leads to the same result).

6. Light curve solution

From the overall photometric data set, a subset of 23 contributions was chosen to create the profile used for the light curve solution. The subsets, marked "used for profile" in Table 1, were selected according to their length, the coverage in phase they contributed to, the filter they were taken in (=none), and their reliability and quality with respect to trends. In contrast to the data shown in Fig. 2, each of the selected data sets was then cleaned from suspicious points and normalised at its maximum. A folded profile with 200 points, with a phase bin width of 0.005 units, and with phase zero set at the minimum of primary eclipse, was then obtained from these data, and a few remaining clearly unreliable points were removed.

This light curve, formed of 187 normal points (in intensity units), normalized to unity outside eclipse, was subjected to a numerical solution by the application of the MORO code (Drechsel et al. 1995). The code is based on the Wilson-Devinney (1971) logistical approach, but incorporates a modified Roche model to account for radiative interaction between the components and uses the SIMPLEX method as parameter optimization algorithm.

The solution mode was chosen such that no a priori restriction of the system configuration was imposed (equivalent to the original Wilson-Devinney mode 2). The total number of light curve parameters for a single passband curve amounts to 17. Since the observed eclipse minimum depth is only moderate (≈16% of maximum light), as no signature of the secondary except its light blocking effect is evident, and because no colour information follows from the white light curve, solutions tend to be underdetermined, especially if the adjustable parameter set is too large. Hence it was important to use any available secondary information from spectroscopy or stellar atmospheres' theory to reduce the number of free light curve parameters and keep some of them at fixed values.

No information at all is available for a possible eccentricity of the orbit, since the position of the unobserved secondary eclipse cannot be determined, and radial velocity measurements do not exist so far. Therefore circular orbits ($e = 0$) and synchronously rotating components were assumed – as is mostly the case in close binary systems due to their very short synchronization time scales. According to the late spectral type, bolometric albedos A_1 and A_2 were fixed at their usually expected values of 0.5 for convective outer layers, and gravity darkening exponents g_1 and g_2 were set to 0.32 as predicted by Lucy's law (1967). Linear limb darkening coefficients are poorly known for very late spectral types. From an extrapolation of the grids of Wade & Rucinski (1985) and Díaz-Cordovés et al. (1995) at their cool ends one obtains approximate values of $x_1 = 0.5$–0.6, which were used in the solutions. Values of x_2 (and g_2) are irrelevant due to the absence of any measurable secondary light.

The primary effective temperature was always fixed at $T_1 = 3000$ K, typical for spectral type M5 V, since the result of $T_{\rm eff} = 4200$ K from the spectral analysis has only become available recently, following the February 2003 OMEGA-Cass observations. This choice is however not critical, because the light curve solution only allows to derive the temperature

Table 5. MORO solutions of the light curve of the eclipsing system 2MASS J0516288+260738.

Parameter	a	b	c	d	e	f	g	h
q (= M_2/M_1)	0.085	0.094	0.110	0.122	0.156	0.181	0.182	0.184
i	75.°5	74.°3	74.°0	73.°9	73.°5	72.°4	72.°9	72.°3
T_1/T_2	1.67	1.72	1.74	1.73	1.77	1.63	1.83	1.88
r_1/r_2^a	1.11	0.89	0.85	0.87	0.85	0.67	0.73	0.64
Ω_1	5.138	5.350	5.510	5.520	5.598	6.123	6.001	6.220
Ω_2	1.961	1.943	1.997	2.055	2.182	2.197	2.236	2.198
L_1^b	0.998	0.998	0.999	0.998	0.999	0.993	0.999	0.999
x_1^c	0.60*	0.60*	0.50*	0.50*	0.60*	0.60*	0.488	0.60*
x_2^c	0.50*	0.50*	0.50*	0.50*	0.50*	0.50*	0.527	0.50*
l_3^d	0%*	0%*	0%*	0%*	0%*	0%*	1.5%	0%*
1σ deviation	0.00750	0.00750	0.00749	0.00749	0.00749	0.00755	0.00750	0.00749

[a] Ratio of mean Roche radii.

[b] Relative luminosity $L_1/(L_1 + L_2)$; L_2 is not independently adjusted, but recomputed from r_2 and T_2.

[c] Linear limb darkening coefficient; theoretical value for V band taken from Díaz-Cordovés et al. (1995).

[d] Fraction of third light at maximum.

* Fixed.

ratio T_1/T_2, and from a single unfiltered curve no colour information can be extracted. The remaining set of adjustable parameters therefore comprised inclination i, mass ratio $q = M_2/M_1$, secondary temperature T_2, surface potentials Ω_1 and Ω_2, primary luminosity L_1, and third light l_3. L_2 was not independently adjusted, but recomputed from T_2 and the secondary surface area over the Planck law. Trial runs showed that the percentage of third light l_3 attributable to a possible unresolved field star tended toward zero (except for solution g, see Table 5), so that this parameter was subsequently fixed at $l_3 = 0$ in the iterations of all other solutions.

Convergent solutions were achieved after numerous trial runs with a variety of start parameter sets (start simplices) and different parameter increments as starting points of the automatic iteration process, which covered essentially the whole range of physically reasonable parameter values. For reasons discussed earlier the numerical process could not be expected to yield a single best and unique solution. Instead, for a couple of comparably good solutions, there was no obvious way to qualify one of these as definitely best representation, as judged from the final standard deviations of normal points from the synthetic curves. To give an impression of the typical scatter of final parameters we present a subsample of 8 different solutions with the relatively best sigma standard deviations in Table 5. These are sorted in a sequence of increasing q values. It is obvious that one can identify two groups of solutions according to the value of the mass ratio: solutions a–d cluster around $q \sim 0.10 \pm 0.02$, while cases e–h yielded $q \sim 0.18 \pm 0.01$.

A common feature of all solutions are consistent values of inclination ($i \sim 72°–75°$), temperature ratio ($T_1/T_2 \sim 1.6–1.8$), ratio of radii (r_1/r_2 around 0.9), extremely low secondary luminosity ($L_2/L_1 \approx 1–2 \times 10^{-3}$), and similar system configuration. As shown for solution c in Fig. 4, which can be considered as representative for the group of solutions with $q \approx 0.1$, the secondary is of about the same size as the primary, and nearly fills its Roche lobe in a close to semi-detached configuration. The photometric determination of T_2 and hence the temperature ratio must be considered very uncertain, because of the missing secondary eclipse and the extreme luminosity ratio.

The overall representation of the observations by the theoretical light curve is very good. Figure 5 (top) displays the normal points in comparison with the synthetic curve (solid line). Especially the eclipse minimum is matched in detail. The standard deviation amounts to only 7.5 mmag, which corresponds to the typical scatter of measurements binned to normal points. As shown in the bottom part of Fig. 5, most observations lie in a 1σ band, and all within a 3σ belt, with no apparent systematic deviations. Figure 6 gives a 3-dimensional impression of the aspects of the system at different phase angles as viewed under an inclination of 74°; the configuration corresponds to the parameters of solution c.

7. Discussion of alternate configurations

The system is located only 6.9° above the galactic plane (in an outward direction). This implies that the reddening through interstellar extinction is potentially very high. Although from spectral observations in conjunction with detailed Galactic extinction models many stellar spectral and luminosity types other than late main sequence stars can be excluded, it is also instructive to make use of the independent information from the light curve solution alone. Through the geometry of the system, and fundamental stellar parameters that cannot be substantially altered even when a star resides in a close binary system, most of the following alternative combinations can be excluded. This in turn justifies the restriction of the discussion in Sect. 5 to a late dwarf system.

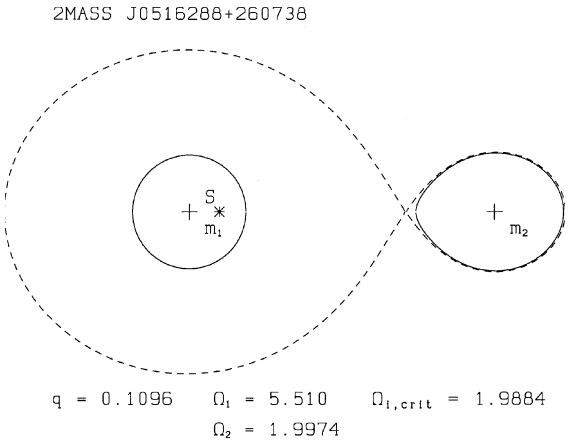

Fig. 4. Meridional intersection of surface and inner critical Roche equipotentials corresponding to the nearly semi-detached system configuration of solution c (see Table 5); the substellar secondary component is close to contact with its Roche lobe.

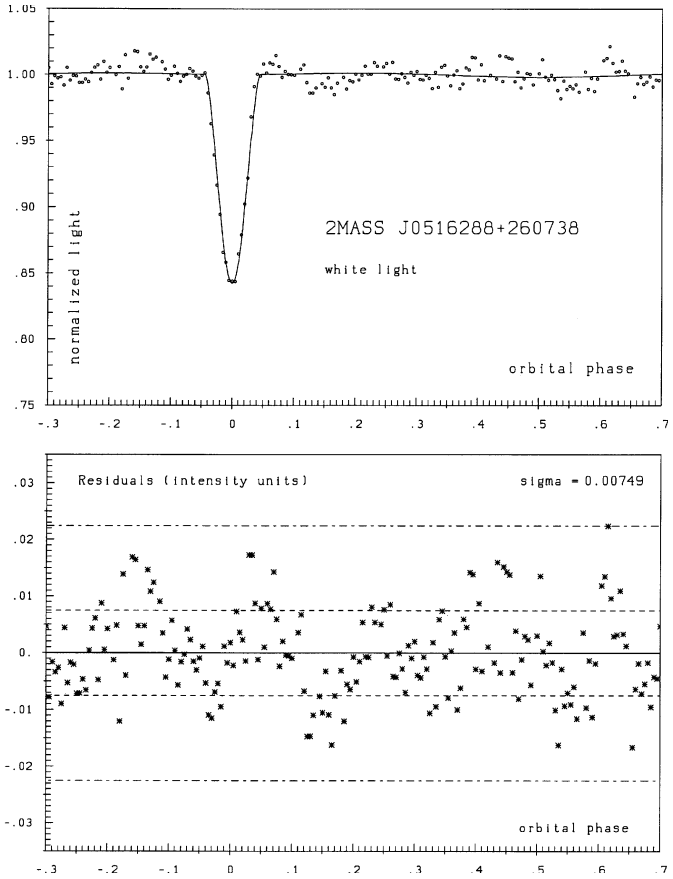

Fig. 5. Top part shows the observed light curve in white light (dots are normal points formed by binning individual observations to phase intervals of width 0.005) together with the theoretical curve (solid line) corresponding to solution c of Table 5; maximum light (intensity) was normalized to unity, and phases were computed according to the ephemeris of Sect. 3.2; bottom part shows residuals of observations (in intensity units) with 1σ and 3σ belts.

7.1. Reddened giant stars

Up to spectral types G5 or earlier, luminosity class III red giants have radii larger than the orbital separation dictated by the measured orbital period and a total mass sum of the system of up to twice their own mass. This is illustrated in Fig. 7: The solid line represents the orbital separation of the system components as a function of the total system mass for the given orbital period of $1\overset{\mathrm{d}}{.}29$. It is therefore a strict upper limit to the radius of any single component of the system. The type III giant star spectral types are printed at the position of their radii, once over their corresponding stellar mass and once at twice that value. These overplotted radii for type III giants were taken from the mass-radius relation by Cox (2000). Using the stellar mass and the double of it means that in between those two values all possible mass combinations are covered, since the roles of primary and secondary would simply become reversed if an even greater fraction of the total mass were attributed to the presumed secondary. The first case represents the limit in which the mass of the companion is negligible, so that the total mass is solely made up of the giant's contribution, while in the second case the mass of the giant amounts to half of the total mass in the system.

In a naïve consideration, the early type giants could fit within the orbital separation, even if it is clear that most of the time they would reach well over half of the total distance. But although these earlier types could just about fit into the system, it can easily be shown that their deformation within the Roche potential would in all cases result in large ellipsoidal light variations, which are not observed in the actual light curve. In addition, the width of the observed eclipse minimum would cover a much broader phase range. For these estimates, the binary eclipse simulation program `nightfall` (R. Wichmann, Landessternware Heidelberg, Germany) which calculates synthetic light curves taking into account the distortion of the stars in Roche geometry was used.

Since these considerations equally apply to luminosity classes II and I, and even in a much stricter form there, the luminosity class for the more luminous object in the system must be V or higher.

7.2. Reddened earlier main sequence stars

Giant stars do not fit within the prescribed orbit; but what about bright early main sequence stars that appear reddened by strong interstellar absorption? Very early main sequence stars have masses and especially radii similar to those of type III giants, so that, as above, geometry arguments can be brought forward to rule out a combination of two very early-type components. This is important, as results from stellar structure will be utilized to find physically meaningful pairs in what follows.

The light curve solutions constrain the mass ratio, the radius ratio and the ratio of the effective temperatures almost regardless of the absolute value of T_1. Using tabulated values for the masses, radii and effective temperatures of stellar and substellar objects, the possible components making up the system can be constrained by requiring that both of them have parameters reasonably close to those of isolated main sequence stars or substellar objects. The stellar parameters used in the following were taken from Cox (2000), those for substellar objects

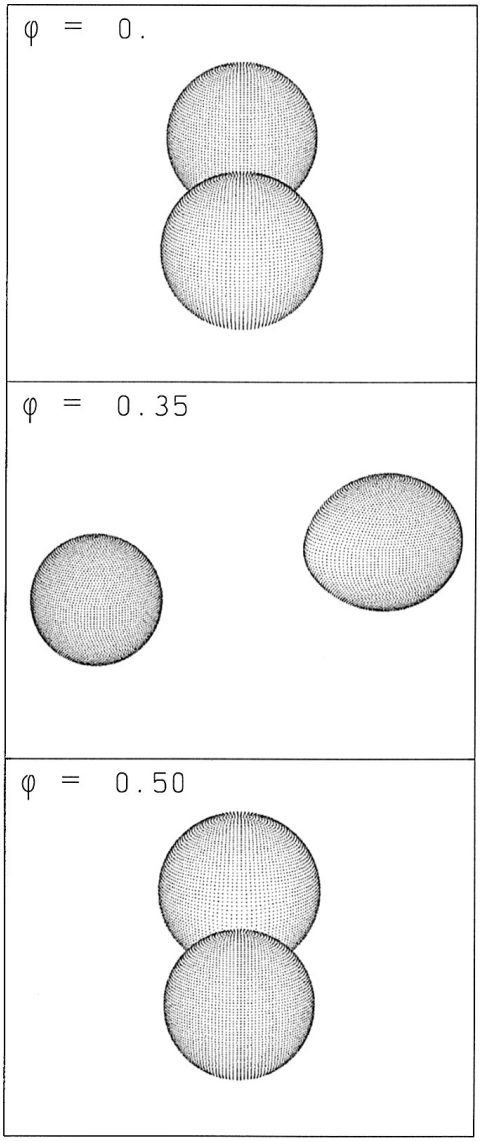

Fig. 6. Aspects of the system at three different phases; viewing angle is 74°, and system parameters correspond to solution c of Table 5.

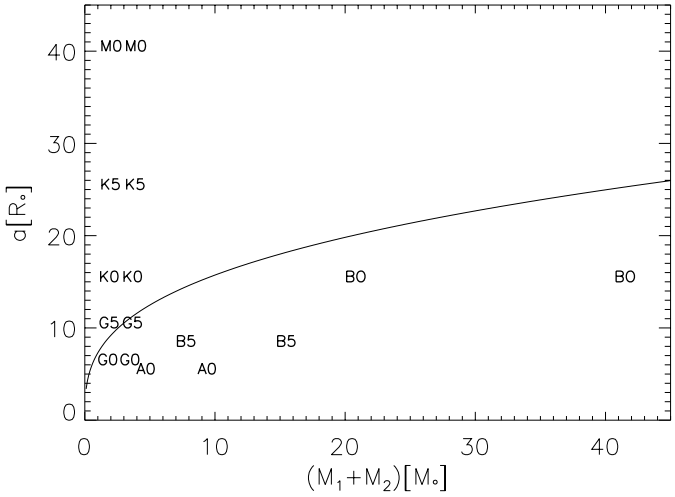

Fig. 7. Orbital separation a as a function of the mass sum $M_1 + M_2$ of the system at the 1.29 d period. Overplotted are radii for type III giants; explanation see text (Sect. 7.1).

(for ages ranging from 1 M yrs to 10 G yrs) from Chabrier et al. (2000) and Baraffe et al. (2002).

The ratios of effective temperatures and masses of the binary components for the light curve solutions c and g from Table 5, which can be considered representative for the two bulges of solutions clustering around $q = 0.10$ and 0.18, are used to find the corresponding effective temperatures and masses of the secondary as a function of primary mass. For all main sequence stars, their effective temperatures and those required by the two representative solutions for the secondary are plotted in Fig. 8. The zero-age main sequence objects and the youngest substellar objects (1 M yrs old) are marked by plus signs and are connected by a thick solid line; higher age substellar models are also represented by plus signs, which remain, however, isolated for clarity. For both solutions a row of squares connected by a solid line is shown. The squares correspond to the locations of the secondary in the $T_{\rm eff} - M$ diagram, which follow from the temperature and mass of a main sequence primary using the temperature and mass ratios of the respective photometric solutions c and g. For each square plotted, the corresponding error estimates from the typical dispersion within each of the two groups are indicated by small dots which represent the end points of the associated error bars (not drawn as full lines to preserve more clarity in this complex representation). For the primary a variety of spectral types between O5 V and M8 V were considered to cover the full zero-age main sequence (plus signs). When inspecting this figure and the following graph, note that the plot scale is logarithmic so that offsets between curves can be much larger in regions of the plot that correspond to the upper main sequence than they might intuitively seem.

The curve for the secondary corresponding to solution c only approaches and intersects the main sequence at its lower end and therefore excludes highly reddened hotter main sequence stars as a possible primary, since the corresponding secondaries cannot exist. The other line corresponding to solution g starts off close to the main sequence and comes back to it earlier than the other one. As stated above, the combination of two upper main sequence stars as a possible solution can be ruled out, because such extended stars could only reside within the given orbit if an appreciable distortion of the primary is allowed for, which would inevitably result in an easily observable ellipsoidal light variation. Apart from this special case for g on the upper main sequence, solutions (discretised in, on average, 5-subclass steps!) were elected possible whenever the error range for such a discrete secondary location intersected the stellar or substellar regime. Errors in parameter ratios are regularly smaller than the discretisation in spectral classes used, so the limits given can be regarded to be accurate to within roughly two subclasses.

On the lower main sequence, the earliest possible spectral types for the primary in the two cases are as listed in the first line of Table 6. In case g, K5 and M0 primaries must be excluded. When the mass-radius relation is taken into account in addition to the just invoked mass-temperature correlation, these

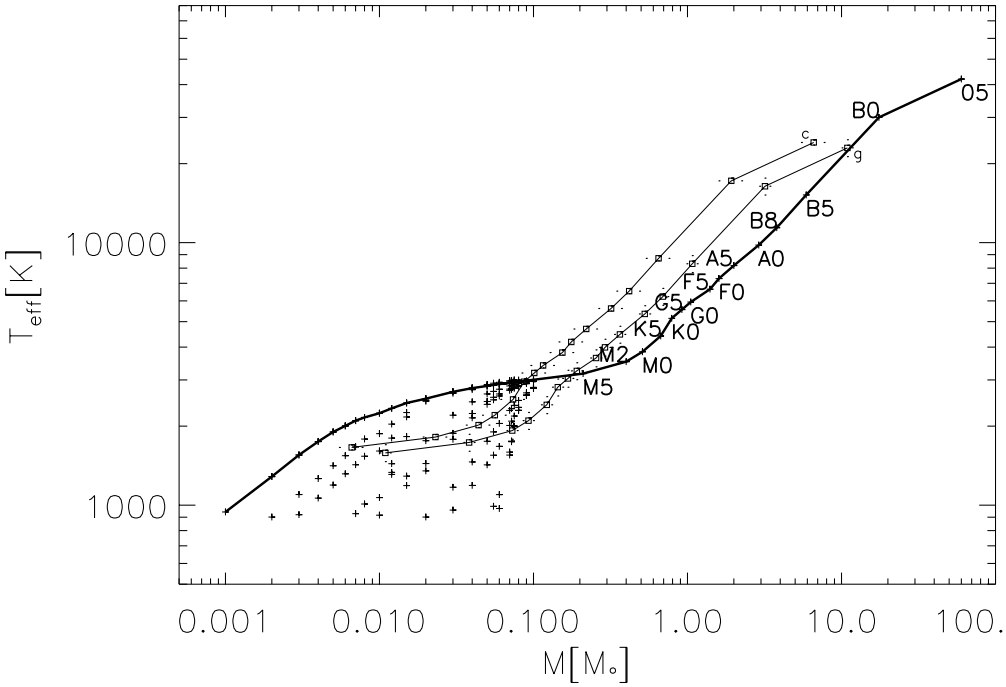

Fig. 8. Effective temperature as a function of the stellar mass for zero-age main sequence stars and substellar objects (plus signs) and their secondaries according to Table 5 (squares); further explanations see text (Sect. 7.2).

Table 6. Interpretation of Figs. 8 and 9; for explanations see Sects. 7.2 and 8.

Possible primary spectral types for solution	Group a–d	Group e–h
From mass-temperature relation (Fig. 8)	upper limit G5	region G0–K0, or upper limit M2
From mass-radius relation (Fig. 9)	upper limit G5	upper limit M0
Combined constraints	upper limit G5	upper limit M2
Consistency with spectroscopy (K7 ± 2)	fully consistent	marginally consistent at most
Resulting secondary mass [$M_\odot$]	upper limit 0.11	upper limit 0.076
Resulting secondary mass [$M_\odot$] for K7	0.062 ± 0.01	0.105 ± 0.01

upper limits can be even further constrained, as will be shown next.

The ratios of radius and mass for the binary components (also taken from Table 5) together with tabulated mass-radius relations from the same sources as above can be subjected to the same procedure. The designations in Fig. 9 are analogous to those in Fig. 8. The results are also compiled in Table 6. The primary can be constrained to be of spectral type G5 or later for solution c, or of spectral type M0 for solution g. The second line in Table 6 lists these limits without any additional age constraints that migth be present (see this discussion later).

Combining the constraints from both Figs. 8 and 9 yields an overall upper limit for each solution as listed in Table 6, line 3. Solution c allows for a primary no earlier than G5, while solution g restricts possible primaries to spectral types no earlier than M2. Spectroscopic results strongly favour the group a–d solution, since the overall constraint of G5 for the primary spectral class is entirely consistent with the conclusion in Sect. 5. For an upper limit of M2, on the other hand, it would be hard to claim consistency with the spectroscopy results. Table 6 nevertheless explores the mass range for the secondary in different scenarios (entries in lines 5 and 6).

An additional constraint not taken into account so far is the age of the system, which for the more likely solutions a-d is restricted to below 0.01 Gyr by the mass-radius relation. A young system is also allowed for by the mass-temperature relation. However, this corresponds to a lifetime of the system in which the K star will not have had enough time to attain the zero-age main sequence yet, and will hence not necessarily have the ZAMS parameters assumed to deduce these constraints in the first place. This might well limit the overall usefulness of this discussion, and is a point that will have to be re-addressed once better data has become available for this object.

7.3. Nearly identical components

A serious objection to the interpretation presented so far emerges if the orbital period is really twice as long as assumed

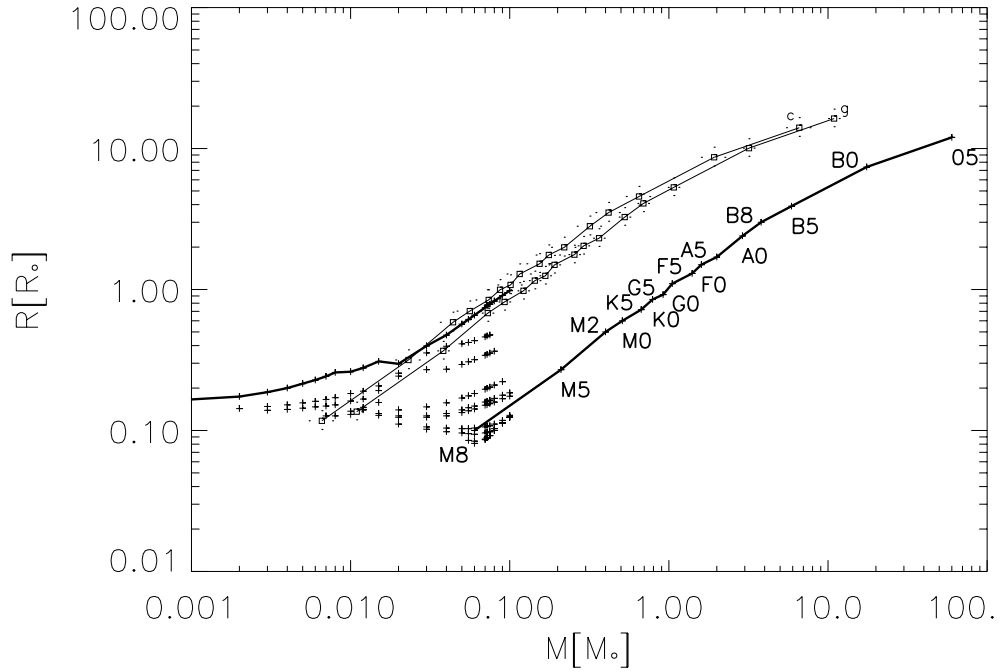

Fig. 9. Mass-radius relation for zero-age main sequence stars and substellar objects (plus signs) and their secondaries according to Table 5 (squares); further explanations see text (Sect. 7.2).

(see a similar initial ambiguity for CM Dra where this indeed turned out to be the correct interpretation in Eggen & Sandage 1967). The eclipse ephemeris given in Sect. 3.2 would then not correspond to the orbital ephemeris of the system any more, as assumed throughout the light curve analysis in Sect. 6. Hence, results obtained there are not applicable to the current discussion, where identical components could then produce undistinguishable primary and secondary eclipses. In many binary systems, the mass ratio is close to one, so this is not an altogether implausible, but from a statistical point of view highly unlikely configuration. This possible complication can currently not be resolved, since the scenario could only be conclusively ruled out, or corrobated, with radial velocity measurements.

7.4. Two old white dwarfs

A further scenario that requires consideration is a system consisting of two old and therefore very red white dwarfs (the effect of interstellar reddening cannot contribute significantly here due to the low intrinsic luminosity of these objects). It is however not very probable that the mass ratio in a double degenerate system is as low as $q \approx 0.1$. For the given period, the duration of eclipse would be of order 10^{-3} phase units, completely incompatible with observations.

8. Conclusion

Despite the remaining uncertainties, from the data presented in this paper it is plausible that the newly discovered eclipsing binary system 2MASS J0516288+260738 consists of a late K-type (pre-)main sequence star as a primary and a substellar object as a secondary. For the spectral class upper limits derived in Sect. 7.2, Table 6 also lists the secondary masses according to the mass ratios given in Table 5 for each solution. All of these mass values, which are close to or below the substellar limit of $0.075\,M_{\odot}$ required for stable hydrogen burning, represent upper limits. Taking into account the additional information available from spectral analysis which favours a spectral type around K7 results in a value of $\approx 0.06\,M_{\odot}$ for the secondary's mass. In this case, only solutions a-d are considered as likely since a spectral type of K7 would not be consistent with solutions e–h. A substellar nature of the companion is therefore quite likely: The unusually low mass ratios in all solutions make the secondary a good Brown dwarf candidate.

This interpretation should now be checked by trying to confirm the spectral classification via the detection of spectral lines in new high resolution, high signal-to-noise optical and/or infrared spectra. These lines could then also be used to obtain radial velocity measurements for the system which should eventually provide absolute masses.

Together with the extensive light curve available, the system has the potential to provide a new high-quality point for the mass-radius relation of the lower main sequence (or for pre-main sequence evolutionary tracks), and the first one obtained from eclipse measurements for a sub-stellar object.

Acknowledgements. The authors would like to thank K. Werner and H. Mauder for helpful discussions and friendly support, and P. A. Woudt for his assistance in obtaining a *V* magnitude for 2MASS J0516288+260738. We also would like to thank R. Gredel for allocating Director's discretionary time and U. Thiele for carrying out the OMEGA-Cass observation at Calar Alto observatory in service mode. We acknowledge the use of the `nightfall` program for light-curve synthesis of eclipsing binaries (`http://www.lsw.uni-heidelberg.de/~rwichman/Nightfall.html`), written by R. Wichmann. Part of this work was supported by the German *Deutsche Forschungsgemeinschaft* under project grants

DR 281/13-1 and DR 281/13-2, as well as under travel grants DR 281/16-1, DR 281/18-1, and NA 365/6-1. The Wise Observatory contribution to this work is supported by the Israel Science Foundation. This research has made use of the USNOFS Image and Catalogue Archive operated by the United States Naval Observatory, Flagstaff Station (http://www.nofs.navy.mil/data/fchpix/).

References

Allard, F., Hauschildt, P. H., Alexander, D. R., Tamanai, A., & Schweitzer, A. 2001, ApJ, 556, 357
Andersen, J. 1991, 3, 91
Andersen, J. 1998, in IAU Symp., 99
Arenou, F., Grenon, M., & Gomez, A. 1992, A&A, 258, 104
Baraffe, I., Chabrier, G., Allard, F., & Hauschildt, P. H. 2002, A&A, 382, 563
Campins, H., Rieke, G. H., & Lebofsky, M. J. 1985, AJ, 90, 896
Cardelli, J. A., Clayton, G. C., & Mathis, J. S. 1989, ApJ, 345, 245
Chabrier, G., Baraffe, I., Allard, F., & Hauschildt, P. 2000, ApJ, 542, 464
Condon, J. J., Cotton, W. D., Greisen, E. W., et al. 1998, AJ, 115, 1693
Cox, A. N. 2000, Allen's astrophysical quantities, 4th ed. (Publisher: New York: AIP Press; Springer), ed. A. N. Cox, ISBN: 0387987460
Delfosse, X., Forveille, T., Beuzit, J.-L., et al. 1999, A&A, 344, 897
Delfosse, X., Forveille, T., Ségransan, D., et al. 2000, A&A, 364, 217
Díaz-Cordovés, J., Claret, A., & Gimenez, A. 1995, A&AS, 110, 329
Drechsel, H., Haas, S., Lorenz, R., & Gayler, S. 1995, A&A, 294, 723
Dreizler, S., Rauch, T., Hauschildt, P., et al. 2002, A&A, 391, L17
Eggen, O. J., & Sandage, A. 1967, ApJ, 148, 911
Grauer, A. D., Wegner, G., Green, R. F., & Liebert, J. 1989, AJ, 98, 2221
Joy, A. H., & Sanford, R. F. 1926, ApJ, 64, 250
Kreysing, H.-C., Brunner, H., & Staubert, R. 1995, A&AS, 114, 465
Lacy, C. H. 1977, ApJ, 218, 444
Leggett, S. K., Allard, F., Geballe, T. R., Hauschildt, P. H., & Schweitzer, A. 2001, ApJ, 548, 908
Leggett, S. K., Hauschildt, P. H., Allard, F., Geballe, T. R., & Baron, E. 2002, MNRAS, 2002, 78
Leung, K.-C., & Schneider, D. P. 1978, AJ, 83, 618
Lucy, L. B. 1967, Z. Astrophys., 65, 89
Ludwig, H.-G., Allard, F., & Hauschildt, P. H. 2002, A&A, 395, 99
Metcalfe, T. S., Mathieu, R. D., Latham, D. W., & Torres, G. 1996, ApJ, 456, 356
Monet, D. G., Levine, S. E., Canzian, B., et al. 2003, AJ, 125, 984
Pounds, K. A., Allan, D. J., Barber, C., et al. 1993, MNRAS, 260, 77
Ribas, I. 2003, A&A, 398, 239
Rieke, G. H., Lebofsky, M. J., & Low, F. J. 1985, AJ, 90, 900
Schmidt-Kaler, T. 1982, in Landolt-Börnstein, Gr. 6, vol. 2b (New York, Berlin, Heidelberg: Springer-Verlag), 1
Schuh, S. L., Dreizler, S., Deetjen, J. L., & Göhler, E. 2003, in Baltic Astronomy, vol. 12, The 6th Whole Earth Telescope Workshop, ed. J.-E. Solheim, & E. Meištas, 167
Ségransan, D., Kervella, P., Forveille, T., & Queloz, D. 2003, A&A, 397, L5
Squires, G. K., Rebull, L. M., Hoard, D., & McCollum, B. 2002, SIRTF Observation Planning Cookbook, version 2.2, [http://sirtf.caltech.edu/SSC/documents/cookbook/html/cookbook.html]
Stoughton, C., Lupton, R. H., Bernardi, M., et al. 2002, AJ, 123, 485
Torres, G., & Ribas, I. 2002, ApJ, 567, 1140
Udalski, A., Paczynski, B., Zebrun, K., et al. 2002a, Acta Astron., 52, 1
Udalski, A., Pietrzynski, G., Szymanski, M., et al. 2003, Acta Astron., 53, 133
Udalski, A., Zebrun, K., Szymanski, M., et al. 2002b, Acta Astron., 52, 115
van Gent, H. 1926, Bull. Astron. Inst. The Netherlands, 3, 121
Wade, R. A., & Rucinski, S. M. 1985, A&AS, 60, 471
Wegner, G., Africano, J. L., & Goodrich, B. 1990, AJ, 99, 1907
Wilson, R. E., & Devinney, E. J. 1971, ApJ, 166, 605

Online Material

Table 1. Photometric observations.

Site	Start time [UT]		Length[h]	Frames	Epoch	Minimum [HJD]	O−C	Comments
SARA	2001 Dec. 06	05:01	7.1	857				used for profile
SARA	2001 Dec. 07	03:14	5.5	664				used for profile
SARA	2001 Dec. 07	10:14	1.9	233				
CAHA	2001 Dec. 07	20:09	8.8	1032	0	2 452 251.5164	−0.0009	used for profile
Piszkéstető	2001 Dec. 07	19:23	7.3	380	0	2 452 251.5164	−0.0009	
BOAO	2001 Dec. 08	11:20	9.0	1029				
Piszkéstető	2001 Dec. 08	18:14	4.7	200				used for profile
WISE	2001 Dec. 09	01:12	2.4	690				used for profile
WISE	2001 Dec. 09	18:02	1.8	511				
Piszkéstető	2001 Dec. 09	18:26	7.5	370				used for profile
WISE	2001 Dec. 09	20:46	2.6	768				used for profile
WISE	2001 Dec. 09	23:43	2.0	564				used for profile
WISE	2001 Dec. 10	01:47	1.8	505				used for profile
BOAO	2001 Dec. 11	16:51	1.6	181				used for profile
BOAO	2001 Dec. 11	19:17	0.9	101				used for profile
SAAO	2001 Dec. 11	22:22	3.0	1080	3	2 452 255.4007	+0.0016	
GAO	2001 Dec. 12	11:33	1.4	308				
SAAO	2001 Dec. 12	21:41	1.7	627				
GAO	2001 Dec. 13	13:47	5.3	1000				
SAAO	2001 Dec. 13	19:57	5.4	1821				
GAO	2001 Dec. 14	12:37	6.7	1301	5			
BOAO	2001 Dec. 14	16:35	2.5	257				used for profile
Piszkéstető	2001 Dec. 14	18:08	6.7	328				used for profile
SAAO	2001 Dec. 14	20:11	5.1	1821				
SAAO	2001 Dec. 15	22:01	1.9	643				
GAO	2001 Dec. 16	16:25	3.2	700				used for profile
SAAO	2001 Dec. 16	19:58	5.3	1901	7			
GAO	2001 Dec. 17	10:51	0.9	203				
GAO	2001 Dec. 17	13:19	0.6	125				
GAO	2001 Dec. 17	15:50	3.2	700				
SAAO	2001 Dec. 17	20:02	5.1	1827				
GAO	2001 Dec. 18	10:22	8.6	1750				
SAAO	2001 Dec. 18	20:03	4.8	1710				
GAO	2001 Dec. 19	12:22	6.7	753	9	2 452 263.1615	−0.0013	used for profile
SAAO	2001 Dec. 19	20:04	4.8	1738				
SARA	2001 Dec. 19	04:54	7.2	817				used for profile
GAO	2001 Dec. 20	10:54	6.2	650				used for profile
SAAO	2001 Dec. 20	19:58	4.9	1752	10	2452264.4599	+0.0031	
SARA	2001 Dec. 20	02:37	9.7	1107				used for profile
SAAO	2001 Dec. 21	19:53	5.0	1804				
GAO	2001 Dec. 22	12:50	6.0	625				used for profile
SAAO	2001 Dec. 22	21:22	3.0	1074				
SARA	2001 Dec. 22	04:31	3.3	404	11	2 452 265.7487	−0.0019	
SARA	2001 Dec. 23	05:12	0.8	100				
SARA	2001 Dec. 23	10:53	1.0	125	12			
GAO	2001 Dec. 23	12:37	5.8	700	12	2 452 267.0450	+0.0004	used for profile
SAAO	2001 Dec. 23	19:54	4.9	1663				
GAO	2001 Dec. 24	12:37	6.0	720				used for profile
CAHA II	2002 Oct. 31	23:11	3.6	50				used for profile
CAHA II	2002 Nov. 04	22:43	1.8	27				used for profile
CAHA II	2002 Nov. 07	02:14	2.4	17	259	2 452 586.6506	+0.0010	
CAHA II	2002 Nov. 09	23:02	6.9	99				Johnson *I* filter data
CAHA II	2002 Nov. 11	22:59	5.2	75	262	2 452 590.5304	−0.0010	Johnson *I* filter data